Calibration and testing with real turbulence of a pyramid sensor employing static modulation

Ledue, Jeffrey; Jolissaint, Laurent; Véran, Jean-Pierre; Bradley, Colin

Publisher's version / Version de l'éditeur:
https://doi.org/10.1364/OE.17.007186
Optics Express, 17, 9, pp. 7186-7195, 2009

Calibration and testing with real turbulence of a pyramid sensor employing static modulation

Jeffrey LeDue[*,1], Laurent Jolissaint[2], Jean-Pierre Véran[2] and Colin Bradley[3]

[1] *Department of Physics and Astronomy, University of Victoria, PO Box 3055 STN CSC, Victoria, BC, V8W 3P6 Canada*
[2] *Herzberg Institute of Astrophysics, National Research Council of Canada, 5071 West Saanich Road, Victoria, BC, V9E 2E7 Canada*
[3] *Department of Mechanical Engineering, University of Victoria PO Box 3055, STN CSC Victoria, BC, V8W 3P6 Canada*
[*] *Current address: School of Optometry, University of California, Berkeley Berkeley CA 94720*
jledue@berkeley.edu

Abstract: The pyramid sensor (PS) is an interesting alternative to the Shack-Hartmann wavefront sensor (SH WFS) for astronomical Adaptive Optics (AO) because of its potential advantages in sensitivity and applicability to novel wavefront sensing schemes. The PS uses a pyramidal prism to perform a knife-edge test in two dimensions simultaneously and relies on modulating the position of the prism to increase the linear dynamic range. It has been suggested that this could also be accomplished by a static diffusing element. We test this idea and show that the diffuser produces a modulation effect. We compare the results of our PS to a SH WFS measuring spatial and temporal properties of real turbulence produced in the lab with a hot-air turbulence generator.

OCIS codes: (010.1080) Active or adaptive optics; (010.7060) Turbulence; (010.7350) Wavefront sensing; (010.1330) Atmospheric turbulence

References and links

1. R. Ragazzoni, "Pupil plane wavefront sensing with an oscillating prism," J. Mod. Opt. **43**, 289–293 (1996).
2. J. M. Beckers, "Adaptive optics for astronomy - Principles, performance, and applications," Annu. Rev. Astron. Astrophys. **31**, 13–62 (1993).
3. R. Ragazzoni and J. Farinato, "Sensitivity of a pyramidic Wave Front sensor in closed loop Adaptive Optics," Astron. Astrophys. **350**, L23–L26 (1999).
4. S. Esposito, A. Riccardi, and O. Feeney, "Closed-loop performance of pyramid wavefront sensor," in *Proc. SPIE Vol. 4034*, pp. 184–189 (2000).
5. S. Esposito and A. Riccardi, "Pyramid Wavefront Sensor behavior in partial correction Adaptive Optic systems," Astron. Astrophys. **369**, L9–L12 (2001).
6. C. Vérinaud, "On the nature of the measurements provided by a pyramid wave-front sensor," Opt. Commun. **233**, 27–38 (2004).
7. A. Riccardi, N. Bindi, R. Ragazzoni, S. Esposito, and P. Stefanini, "Laboratory characterization of a Foucault-like wavefront sensor for adaptive optics," in *Proc. SPIE Vol. 3353*, pp. 941–951 (1998).
8. S. Esposito, O. Feeney, and A. Riccardi, "Laboratory test of a pyramid wavefront sensor," in *Proc. SPIE Vol. 4007*, pp. 416–422 (2000).
9. R. Ragazzoni, A. Ghedina, A. Baruffolo, E. Marchetti, J. Farinato, T. Niero, G. Crimi, and M. Ghigo, "Testing the pyramid wavefront sensor on the sky," in *Proc. SPIE Vol. 4007*, pp. 423–430 (2000).

#108065 - $15.00 USD Received 26 Feb 2009; revised 11 Apr 2009; accepted 13 Apr 2009; published 15 Apr 2009

10. A. Ghedina, M. Cecconi, R. Ragazzoni, J. Farinato, A. Baruffolo, G. Crimi, E. Diolaiti, S. Esposito, L. Fini, M. Ghigo, E. Marchetti, T. Niero, and A. Puglisi, "On Sky Test of the Pyramid Wavefront Sensor," in *Proc. SPIE Vol. 4839*, pp. 869–877 (2003).
11. J. B. Costa, S. Hippler, M. Feldt, S. Esposito, R. Ragazzoni, P. Bizenberger, E. Puga, and T. F. E. Henning, "PYRAMIR: a near-infrared pyramid wavefront sensor for the Calar Alto adaptive optics system," in *Proc. SPIE Vol. 4839*, pp. 280–287 (2003).
12. J. B. Costa, M. Feldt, K. Wagner, P. Bizenberger, S. Hippler, H. Baumeister, M. Stumpf, R. Ragazzoni, S. Esposito, and T. Henning, "Status report of PYRAMIR: a near-infrared pyramid wavefront sensor for ALFA," in *Proc. SPIE Vol. 5490*, pp. 1189–1199 (2004).
13. R. Ragazzoni, "Adaptive optics for giant telescopes: NGS vs. LGS," in *Proceedings of the Backaskog workshop on extremely large telescopes*, pp. 175–180 (2000).
14. R. Ragazzoni, J. Farinato, and E. Marchetti, "Adaptive optics for 100-m-class telescopes: new challenges require new solutions," in *Proc. SPIE Vol. 4007*, pp. 1076–1087 (2000).
15. E. Diolaiti, R. Ragazzoni, and M. Tordi, "Closed loop performance of a layer-oriented multi-conjugate adaptive optics system," Astron. Astrophys. **372**, 710–718 (2001).
16. J. M. Beckers, "Increasing the Size of the Isoplanatic Patch with Multiconjugate Adaptive Optics," in *Proceedings of a ESO Conference on Very Large Telescopes and their Instrumentation, held in Garching, March 21-24, 1988, Garching: European Southern Observatory,* , pp. 693–703 (1988).
17. J. M. Beckers, "Detailed compensation of atmospheric seeing using multiconjugate adaptive optics," in *Proc. SPIE Vol. 1114*, pp. 215–217 (1989).
18. R. Ragazzoni, E. Diolaiti, J. Farinato, E. Fedrigo, E. Marchetti, M. Tordi, and D. Kirkman, "Multiple field of view layer-oriented adaptive optics. Nearly whole sky coverage on 8 m class telescopes and beyond," Astron. Astrophys. **396**, 731–744 (2002).
19. D. Peter, M. Feldt, B. Dorner, T. Henning, S. Hippler, and J. Aceituno, "PYRAMIR: Calibration and Operation of a Pyramid Near-Infrared Wavefront Sensor," Publ. Astron. Soc. Pac. **120**, 872–886 (2008). 0808.0137.
20. R. Ragazzoni, E. Diolaiti, and E. Vernet, "A pyramid wavefront sensor with no dynamic modulation," Opt. Commun. **208**, 51–60 (2002).
21. O. Keskin, L. Jolissaint, C. Bradley, S. Dost, and I. Sharf, "Hot-air turbulence generator for multiconjugate adaptive optics," in *Proc. SPIE Vol. 5162*, pp. 49–57 (2003).
22. O. Keskin, L. Jolissaint, and C. Bradley, "Hot-air optical turbulence generator for the testing of adaptive optics systems: principles and characterization," Appl. Opt. **45**(20), 4888–4897 (2006).
23. Rayleigh, "On methods for detecting small optical retardations, and on the theory of Foucault's test," Philos. Mag. **33**, 161–178 (1917).
24. E. H. Linfoot, "A Contribution to the Theory of the Foucault Test," Proceedings of the Royal Society of London. Series A, Mathematical and Physical Sciences **186**, 72–99 (1946).
25. E. H. Linfoot, "On the theory of the Zonal Foucault Test," Monthly Notices of the Royal Astronomical Society **108**, 428–445 (1948).
26. E. H. Linfoot, "On the Interpretation of the Foucault Test," Proceedings of the Royal Society of London. Series A, Mathematical and Physical Sciences **193**, 248–259 (1948).
27. J. B. Costa, R. Ragazzoni, A. Ghedina, M. Carbillet, C. Vérinaud, M. Feldt, S. Esposito, E. Puga, and J. Farinato, "Is there need of any modulation in the pyramid wavefront sensor?" in *Proc. SPIE Vol. 4839*, pp. 288–298 (2003).
28. J. B. Costa, M. Stumpf, and M. Feldt, "Testing a nonmodulated pyramid wavefront sensor," in *Proc. SPIE Vol. 5490*, pp. 1304–1314 (2004).
29. P. Pugh, D. Lobb, D. Walker and T. Williams, "Pupil-imaging wavefront gradient sensor," Proc. SPIE **2534**, 312–317 (1995).
30. R. Clare and R. Lane, "Comparison of wavefront sensing with the Shack-Hartmann and pyramid sensors," Proc. SPIE **5490**, 1211–1222 (2004).
31. R. J. Noll, "Zernike polynomials and atmospheric turbulence," J. Opt. Soc. Am. **66**, 207–211 (1976).
32. D. M. Winker, "Effect of a finite outer scale on the Zernike decomposition of atmospheric optical turbulence," J. Opt. Soc. Am. A **8**, 1568–1573 (1991).
33. Andrews,L. C., "An analystical model for the refractive index power spectrum and its application to optical scintillations in the atmosphere," J. Mod. Opt. **39**, 1849–1853 (1992).
34. E. Masciadri and J. Vernin, "Optical technique for inner-scale measurement: possible astronomical applications," Appl. Opt. **36**, 1320–1327 (1997).
35. A. Fuchs, M. Tallon, and J. Vernin, "Focusing on a Turbulent Layer: Principle of the "Generalized SCIDAR"," Publ. Astron. Soc. Pac. **110**, 86–91 (1998).
36. Innocenti,C. and Consortini,A. , "Estimate of characteristics scales of atmospheric turbulence by thin beams: comparison between the von Karman and Hill-Andrews models," J. Mod. Opt. **51**, 333–342 (2004).
37. R. Tyson, *Principles of Adaptive Optics*, 2nd ed. (Academic press, 1998).

#108065 - $15.00 USD Received 26 Feb 2009; revised 11 Apr 2009; accepted 13 Apr 2009; published 15 Apr 2009

1. Introduction

The Pyramid Sensor (PS) was proposed in 1996 as an alternative to the more conventional Shack-Hartmann (SH) wavefront sensor (WFS) as a WFS for astronomical adaptive optics (AO). [1] There has been much interest in the device because the PS uses fewer guide star (GS) photons to make the WFS measurements than the SH WFS meaning that a fainter guide star (larger magnitude) can be used to operate the AO system. Since there are few GS's bright enough to provide AO correction, this gain in limiting magnitude addresses one of the main limitations of astronomical AO: a limited number of accessible astronomical targets of interest (low sky coverage). [2] The magnitude gain of the PS has been studied by several authors[3, 4, 5, 6], and the value calculated using a detailed analytic Fourier optics model [6] is 2.2 magnitudes for a 100 m telescope primary and 1.6 magnitudes for a 10 m telescope. The promise of this device to increase the effectiveness of AO systems has led to laboratory experiments[7, 8], on-sky tests[9, 10] and the PYRAMIR WFS upgrade to the AO system ALFA on the 3.5 m telescope at Calar Alto. [11, 12]

The PS is based on the Foucault knife-edge test and because the WFS signals are derived from pupils re-imaged onto a detector, the PS is particularly well suited to the optical co-addition implementation of the Layer-Oriented[13, 14, 15] (LO) variant of Multi-conjugate Adaptive Optics (MCAO)[16, 17] as well as the multiple field-of-view LO-MCAO technique. [18] All of these AO modes can be implemented by optically combining, on a CCD detector, the light coming from multiple GS references corresponding to multiple pyramids. Thus, the PS is a device that has potential advantage in limiting magnitude over the SH WFS and facilitates novel MCAO modes.

However, since the PS is based on the knife-edge test, it yields only the sign of the wavefront slope and it relies on a technique known as modulation to provide linear measurements of the wavefront slope. [1, 7] It was initially suggested that this could be accomplished by oscillating the prism. [1] This is how the PS on-sky at the Italian Telescopio Nazionale Galileo is implemented. [9, 10] PS's have also been implemented in the lab using a tip-tilt mirror for modulation [7, 8] and PYRAMIR also uses this method. [11, 12, 19] It has also been suggested that it may be possible to provide a modulation effect in a static fashion with a diffusive optical element, such as a rough piece of glass, an array of micro-lenses, a phase grating, or a holographic diffuser. [20] In this paper we discuss the results of calibrating a PS implemented using a holographic diffuser (Light Shaping Diffuser from Physical Optics Corporation). We also show a comparison between the PS and a SH WFS (mini-Wavescope from Adaptive Optics Associates) in measuring the spatial and temporal properties of turbulence generated by our hot-air turbulence generator (turbulator). [21, 22] Measurements of the inner and outer scale, the Fried parameter, and the effective wind speed of the turbulence are given.

2. Modulation and the pyramid sensor

Figure 1 shows a schematic diagram of the PS implemented in 1d to demonstrate the principle. The aberrated beam is refocused onto the apex of the prism which spatially filters the electric field phasor in the focal plane. The pupils are re-imaged onto the detector by another lens. The signals are derived from the intensity in the re-imaged pupils. Following the notation of Vérinaud, 2004 the signal derived from the reimaged pupils is given by

$$S(x,y) = \frac{\left|U_p^+(x,y)\right|^2 - \left|U_p^-(x,y)\right|^2}{|A|^2} \tag{1}$$

where $\left|U_p^{\pm}(x,y)\right|^2$ are the intensity in the upper and lower pupils respectively and the signal is normalized by the total intensity, $|A|^2$. The diffraction theory of the Foucault knife-edge

#108065 - $15.00 USD Received 26 Feb 2009; revised 11 Apr 2009; accepted 13 Apr 2009; published 15 Apr 2009

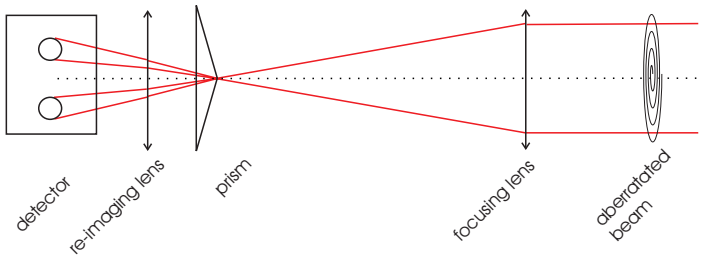

Fig. 1. A schematic diagram of the PS implemented in 1d is shown. The prism spatially filters the electric field phasor of the aberrated beam in the focal plane while splitting the light into two beams. The images of the pupils are formed on the detector by a second lens. The signals are generated by the difference of the illumination in the top and bottom pupil, normalized to the total intensity.

test[23, 24, 25, 26] gives the expression for the illumination in the re-imaged pupils

$$U_p^{\pm}(x,y) = \frac{1}{2}E(x,y) \mp \frac{i}{2\pi}\int_{-\infty}^{\infty}\frac{E(t,y)}{t-x}dx \tag{2}$$

and can be used to model the PS in 1d in the limit of small phase aberrations for an infinite aperture. [6] The Fourier transform of the PS signals is given by

$$S = \begin{cases} -isgn(f) & |f| > \frac{\alpha}{\lambda} \\ -\frac{i\lambda}{\alpha}f & |f| < \frac{\alpha}{\lambda} \end{cases}$$

where α is the modulation angle and f is the spatial frequency. The result shows two distinct behaviors. [6] For $f < \alpha/\lambda$ the sensor signal in the Fourier domain is proportional to the spatial frequency indicating that the PS acts as a slope sensor. In the regime $f > \alpha/\lambda$, the PS behaves as a phase sensor. [6] Thus, the size of the modulation angle determines the dynamic range over which the PS gives a linear response to tilt.

As mentioned in the introduction there are several different options for modulation. The two methods of dynamic modulation, oscillation of the pyramid and tip-tilt mirror, are quite similar. In the first scenario the pyramid is moved around in the focal spot at its apex at a rate exceeding the frame rate of the PS detector. [1] In the case of tip-tilt modulation, a tip-tilt mirror is inserted into the optical path in a plane conjugate to the entrance pupil and the PS detector. The beam is then steered such that the focal point moves around the four facets of the pyramid, again at a rate exceeding the frame rate of the detector. [7] Considering the effect geometrically, if the displacement of the pyramid or focal spot is larger than the largest transverse deviation of a ray from the paraxial focus then the ray will spend some time on each facet. Thus, the PS signals generated from the intensity in the detector plane will be proportional to the ray deviation and hence the tilt in the entrance pupil and this is how modulation was originally presented. [1, 7, 8] Static modulation provides the same effect, but with no moving parts. A light diffusing element is placed in the optical path and serves to create a blur spot on the apex of the prism. The size of this blur spot is proportional to the diffusing angle of the element and modulation using this scheme has been shown to be entirely equivalent to the dynamic case by means of an analytic model. [20] It has the advantage over dynamic modulation that the optical design is facilitated without the active elements. For the multi-reference wavefront sensing applications outlined above, it is particularly advantageous to have static diffusing elements as the number of active

#108065 - $15.00 USD Received 26 Feb 2009; revised 11 Apr 2009; accepted 13 Apr 2009; published 15 Apr 2009

elements required scales with the number of GS's. In addition to the static technique, it has been proposed that residual aberration while an AO system is running in closed loop may provide modulation[27] and studies of this idea are ongoing. [28] This is an attractive idea as well because for astronomical AO applications it removes the necessity for modulation altogether; however, it may be advantageous to employ static modulation to enable the PS to better cope with the effects of telescope jitter and reduce the manufacturing tolerances on the pyramid apex.

On the other hand, static modulation fixes the sensitivity of the PS as the blur spot on the apex of the prism is determined by whichever diffusive element is chosen. The capacity to dynamically adjust the sensitivity of the PS by changing the modulation amplitude is one advantage of the PS over a SH WFS. [1] However, holographic diffusers with a gradient of diffusing angle are commercially available (Physical Optics Corporation) and with the reintroduction of a moving part, such as a motorized linear translator, variable sensitivity is maintained with less complexity than a tip-tilt mirror or an oscillating prism.

3. Experiment

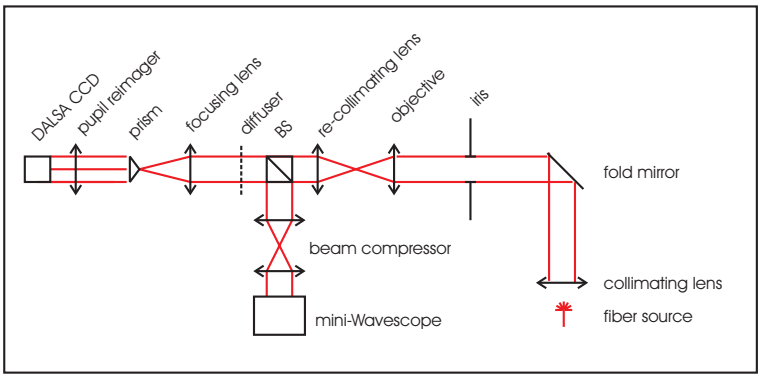

Fig. 2. A schematic diagram of the experimental setup is shown. Light from a fiber source is collimated and a tilt is introduced by the fold mirror. Using the beamsplitter the tilt was measured by the mini-Wavescope and the intensity in the re-imaged pupil of the PS was recorded. The turbulator was introduced into the setup by replacing the fold mirror and repositioning the source in line with the PS CCD.

We have implemented the PS in 1d using a prism as opposed to the 2d version using a four faceted pyramid. The underlying principles are the same in both cases and this implementation allows us to test the static modulation idea without the complications associated with manufacturing a pyramid. A sensor based on crossed prisms [29] or a lenslet array sampling the focal plane [30] would provide complete 2d gradients without the need for a pyramid however the 1d sensor we have implemented here minimizes complexity while capturing the essential features.

The setup used to calibrate the PS is shown schematically in Fig. 2. A laser diode source (Toshiba TOLD9215 laser diode, Seastar Optics LD-2310 laser diode driver, Seastar Optics AC-9400 power unit) is coupled to an optical fiber and collimated. The beam is reflected from a fold mirror, and passes through an iris with a diameter of 1.65 cm, which is the stop of the system. The light then passes through the objective lens which simulates the telescope aperture and is re-collimated after the telescope focal plane. The beam is then split and one arm proceeds to the PS, where it passes through a diffusing element (Light Shaping Diffuser, Physical Optics Corporation) and is refocused, spatially filtered by the prism and the pupil is re-imaged onto the detector (DALSA CA-D1-0128A CCD and BitFlow Roadrunner Framegrabber). The other arm

#108065 - $15.00 USD Received 26 Feb 2009; revised 11 Apr 2009; accepted 13 Apr 2009; published 15 Apr 2009

of the beam passes through a 2x beam compressor and then to the mini-Wavescope (SH WFS from Adaptive Optics Associates).

In order to calibrate the PS's response as a slope sensor, a tilt is introduced using the fold mirror and measured using the mini-Wavescope while the corresponding re-imaged pupil is recorded on the PS camera. The relative change in intensity as a function of tilt is calculated over the whole re-imaged pupil or for any grid of subapertures. The calibration curves are shown in Fig. 3 and discussed in section 4 below.

For the measurement of turbulent wavefronts produced by the turbulator, the setup was modified such that the fold mirror was removed and the source was placed in line with the PS CCD. The turbulator was placed between the source and the iris which remains the stop of the system. The turbulator operates by mixing two streams of air, one warm and one cool, to produce optical turbulence due to the temperature dependence of the index of refraction. The user has control over the speed of the fans (wind speed) and the temperature difference between the two streams of air. Data was collected for a variety of temperature differences for a constant fan speed.

The wind speed of the turbulence was calculated from the temporal power spectra of the measured tilts. The temporal power spectra were calculated as the Fourier transform of the autocorrelation of the time series of tilts measured with each sensor. For spatial characterization using the mini-Wavescope, the variances of the Zernike coefficients of an expansion of the reconstructed wavefront are compared to the diagonal of the Zernike-Komolgorov Covariance matrix [31] modified by the attenuation due to the outer[32] and inner scale, as in the Hill-Andrews model.[33] In the case of the PS a mask is applied to raw image from the CCD camera to isolate the re-imaged pupil. The pupil is then divided into subapertures and the intensity in each subaperture is related to the tilt by the calibration constant generating a map of the local slope of the wavefront orthogonal to the apex of the prism. The slope of the wavefront is then projected onto the Zernike basis and the variance of the coefficients of the expansion are compared to those calculated using the Zernike-Komolgorov Covariance matrix and the Zernike Derivative matrix [31].

4. Results

Figure 3 shows the response of the 1d PS to the incoming tilt. The two curves represent a 0.5° diffuser and 1.0° diffuser. In the case of static modulation using a diffuser, the diffusion angle is the modulation angle and the angles used here are sufficiently large for the PS to operate only in the linear regime. The curves are remarkably linear and the slopes are 1.62 ± 0.03 mrad^{-1} and 0.89 ± 0.01 mrad^{-1} respectively. The sensitivity is roughly a factor of two lower for the 1.0° diffuser as it produces a blur spot on the PS apex which is larger by the same factor. The use of the diffuser clearly results in a linear response of the intensity in the re-imaged pupil to an incoming tilt. This directly demonstrates that modulation can be achieved with a static diffusing element. The 0.5° diffuser was used to make the measurements of the turbulent wavefronts produced by the turbulator.

Figure 4 shows the temporal power spectra of tilt calculated for the PS and the mini-Wavescope at $\Delta T \sim 140^\circ$C. The power spectra have characteristic high and low frequency slopes on a log scale and the transition frequency (f_{knee}) is related to the average wind speed by

$$f_{knee} = 0.3 \frac{v_{eff}}{D} \tag{3}$$

The DALSA CCD of the PS achieves an average frame rate of 522 Hz and the mini-Wavescope is based on a Pulnix CCD which operates at 30 Hz. The temporal properties agree well for all of the measured temperature differences up to 15 Hz where we can compare the sensors.

#108065 - $15.00 USD Received 26 Feb 2009; revised 11 Apr 2009; accepted 13 Apr 2009; published 15 Apr 2009

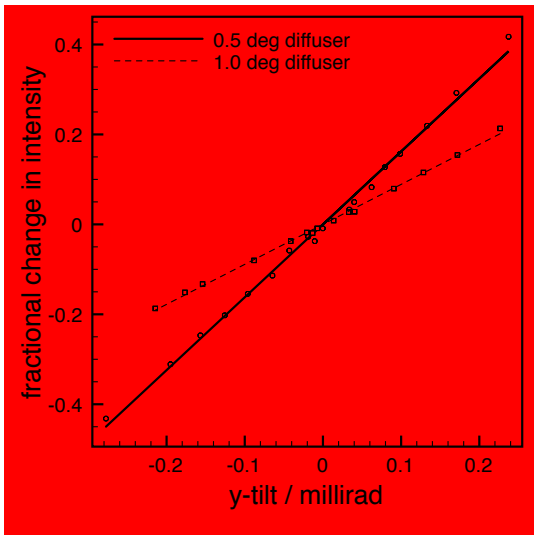

Fig. 3. This plot shows the fractional change in intensity in the re-imaged pupil of the PS recorded with the DALSA CCD. The x and y error bars are less than or equal to the size of the data points. The slope of calibration curve for the 0.5° diffuser is 1.62 ± 0.03 millirad^{-1} and 0.89 ± 0.01 millirad^{-1} for the 1.0° diffuser. The linearity of the tilt response demonstrates the modulation effect provided by the diffuser and the fact that the slope decreases when the modulation angle is increased illustrates that the sensitivity of the PS is inversely proportional to the modulation angle.

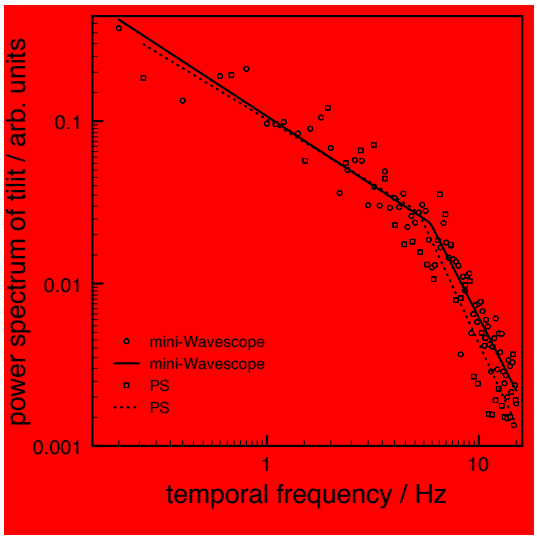

Fig. 4. This plot shows the temporal power spectra of the tilt mode of the turbulence produced by the turbulator calculated using the mini-Wavescope and PS data at a temperature difference of $\Delta T \approx 140^{\circ}$C. Fitting was performed to extract the knee frequency at the transition between the low frequency and high frequency regimes. This frequency is related to the effective wind speed, v_{eff}, of the turbulator by equation 3.

#108065 - $15.00 USD Received 26 Feb 2009; revised 11 Apr 2009; accepted 13 Apr 2009; published 15 Apr 2009

The low and high frequency slope for the mini-Wavescope data are -0.9 ± 0.3 and -2.5 ± 0.8 which agree with the PS values of -0.8 ± 0.2 and -2.8 ± 0.4 respectively. The wind speed derived from the transition frequency above gives 0.276 ± 0.006 m/s for the mini-Wavescope and 0.261 ± 0.008 m/s for the PS. These results show that the two sensors estimate the same temporal properties of the turbulence.

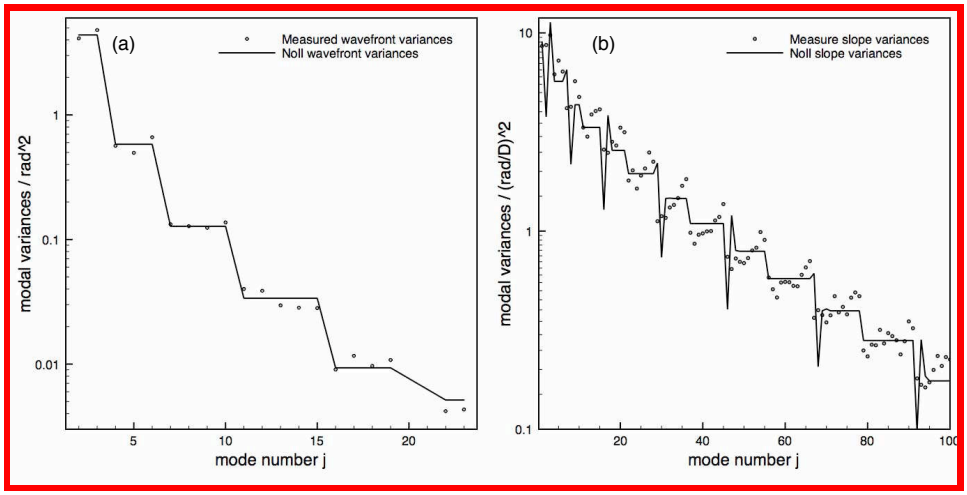

Fig. 5. In (a) the variances of the Zernike wavefront coefficient measured with the mini-Wavescope are shown. The results of Noll, 1976 were modified to included the attenuation of the inner and outer scale and the values for r_0, l_0, and L_0 were extracted by fitting the modified variances. Panel (b) shows the Zernike slope variances measured with the PS. Again fitting is used to obtain r_0, l_0, and L_0.

In order to compare the sensors' spatial characterization of the wavefront we estimate the Fried parameter, r_0, the outer scale, L_0, and the inner scale, l_0. The mini-wavescope software does a reconstruction of the wavefront and a projection onto Zernike modes. The variance of the Zernike coefficients of the wavefront are calculated from the time series of measured coefficients and fit to the expected theoretical values from the Hills-Andrew model giving estimates for r_0, L_0, and l_0. This is shown in Fig. 5(a). The values for r_0, L_0, and l_0 are 3.40 ± 0.03 mm, 170 ± 10 mm, and 11.57 ± 0.07 respectively where the error is that given by χ^2 minimization and estimated from the error on the variance of the coefficients. For the PS, we have 1d sensor and forgo the wavefront reconstruction. Instead the wavefront *slope* is projected onto Zernike modes and the variance of these coefficients is calculated from the measured time series. At this point a similar fit is performed to the expected values of the coefficients of the wavefront *slope* including the damping effects of the inner and outer scale again using the Hill's-Andrew model. The PS case is shown in Fig. 5(b) and the values of r_0, L_0, and l_0 are 2.55 ± 0.08 mm, $70. \pm 9$ mm, and 4.6 ± 0.1 mm. Both sensors, although estimating slightly different parameters, are consistent with other spatial characterizations hot-air turbulence generators. [21, 34, 35, 36]

The Fried parameter is expected to be proportional to $\Delta T^{-6/5}$. The relationship between r_0 and the refractive index structure constant, C_N^2, is given by

$$r_0^{-\frac{5}{3}} = 0.4234 \left(\frac{2\pi}{\lambda}\right)^2 C_N^2 \Delta h \tag{4}$$

where the usual integral over the C_N^2 profile has been replaced by the constant $C_N^2 \Delta h$. [37] $C_N^2 \Delta h$ is proportional to ΔT^2 by Gladstone's law [21] and thus the expected dependence of the

#108065 - $15.00 USD Received 26 Feb 2009; revised 11 Apr 2009; accepted 13 Apr 2009; published 15 Apr 2009

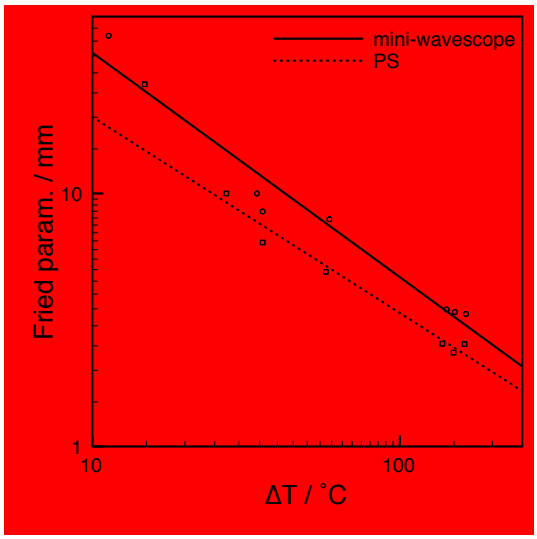

Fig. 6. This plot shows the dependence of r_0 on ΔT observed with the mini-Wavescope and the PS. The lines represent power law fits to the data with a fitting function of the form $r_0 = A\Delta T^{-b}$. The fit parameters are $\log(A) = 2.44 \pm 0.11$ and $b = 0.89 \pm 0.08$ for the mini-Wavescope and $\log(A) = 2.36 \pm 0.13$ and $b = 0.91 \pm 0.09$ for the PS. The exponent, b, agrees well between the two sensors meaning that both WFS's measure the same trend in r_0 vs ΔT

Fried parameter is $r_0 \propto \Delta T^{-6/5}$. However, it has been observed that $C_N^2 \Delta h$ depends linearly on ΔT in the turbulator [21] and in this case $r_0 \propto \Delta T^{-3/5}$. The Fried parameter was measured for several temperature differences (by the procedure described above) and Fig. 6 shows a comparison of the results for both sensors. Power law fits to the data give an exponent of $b = 0.89 \pm 0.08$ and $b = 0.91 \pm 0.09$ for the mini-Wavescope and PS respectively. The two sensors agree and the exponent is between the $-6/5$ and $-3/5$ mentioned above. The PS does, however, systematically underestimate r_0 compared to the mini-Wavescope.

The PS may be systematically underestimating r_0 due, in part, to the way in which the diffuser works. The diffuser is designed to induce a Gaussian blur corresponding to its diffusion angle on a beam which fills its clear aperture ($\sim$25 mm). For a given pencil of rays corresponding to each subaperture the effect of the diffuser may be a slightly more or less than the overall diffusion angle. This implies that the sensitivity of the PS varies with each subaperture. This is in fact the case and Fig. 7 shows a histogram of the measured sensitivities for the PS subapertures. The distribution has a mean value of 1.76 mrad^{-1} close to the global calibration constant of 1.62 mrad^{-1}. The standard deviation of the sensitivity is 0.9 mrad^{-1}. The variation of sensitivity would appear in the wavefront slope measurements as a high order aberration and thus systematically serve to reduce r_0. The sensitivity of a given subaperture depends on the alignment of the system and due to the practical necessity to make adjustments to our prototype sensor, the subaperture sensitivities changed from run to run unlike the global calibration constant which is virtually independent of alignment. This effect could be calibrated out in future work with a re-designed, second generation sensor.

Systematic effects are also apparent in Fig. 5(b). The parameters of the turbulence (r_0, L_0, and l_0) are related to the overall shape and magnitude of the curve and the PS gives reasonable estimates for these. However, with each distinct drop in variance with increasing mode number in the theoretical curve the PS tends to underestimate and then overestimate the variances for

#108065 - $15.00 USD Received 26 Feb 2009; revised 11 Apr 2009; accepted 13 Apr 2009; published 15 Apr 2009

the next few modes leading up to the next sharp decrease. The origin of this effect is not clear and requires further study to determine if it is an artifact of the diffuser used in this study or common to every implementation of static modulation.

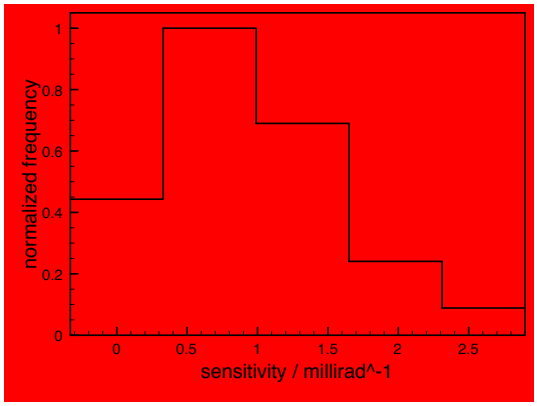

Fig. 7. The distribution of sensitivity values for the PS using a diffuser is shown in this histogram. The mean value is 1.76 mrad^{-1}, close to the overall calibration constant of 1.62 mrad^{-1} from Fig. 3. The standard deviation is 0.9 mrad^{-1}.

5. Conclusion and outlook

We have demonstrated that a light diffusing element provides static modulation in the PS as suggested by Ragazzoni et al., 2002. Sensitivity of the sensor in this configuration varies inversely with the diffusing angle as expected. The PS employing the diffuser and a SH WFS have been used to measure real turbulence, produced by a hot-air turbulence generator. The average effective wind speed measured by the SH WFS is 0.276 ± 0.006 m/s and 0.261 ± 0.008 m/s for the PS. The trend in r_0 observed with the PS compares well to that measured by the SH WFS displaying the expected power law dependence on ΔT. The r_0 values observed with the PS are consistently lower than those of the SH WFS, which we believe to be due to variations in the sensitivity over the pupil of the PS due to the diffuser. This effect will be calibrated out in future work. Overall the spatial characterization of the turbulence with both sensors compare well to the expected range from other characterizations of hot air turbulence generators available in the literature.

#108065 - $15.00 USD Received 26 Feb 2009; revised 11 Apr 2009; accepted 13 Apr 2009; published 15 Apr 2009